Int. J. Ion Mobil. Spec. (2017) 20:57–66
https://doi.org/10.1007/s12127-017-0224-9

ORIGINAL RESEARCH

Construction and evaluation of a hermetically sealed accurate ion mobility instrument

Brian C. Hauck[1,2] · **William F. Siems**[1] · **Charles S. Harden**[3,4] · **Vincent M. McHugh**[5] · **Herbert H. Hill Jr**[1]

Received: 25 September 2017 / Revised: 6 October 2017 / Accepted: 6 October 2017 / Published online: 14 October 2017

Abstract Ion mobility spectrometry (IMS) is widely used to detect and identify chemical warfare agents, narcotics, and explosives in the field based on their reduced mobility (K_0) values. Current detection windows for these analytes can only be as narrow as ±2% of the K_0 values for the analyte being sought. These wide detection windows cause false positive alarms when an interferent with a similar reduced mobility falls within the detection window and triggers an alarm. This results in the loss of time and money as resources are diverted to verify the alarm. A high rate of false positive alarms is caused by a discrepancy in the reported K_0 values across the literature that is, at best, ± 2% of the average available values. By accurately and precisely measuring the variables affecting an ion's K_0 value, an accurate K_0 value can be produced and the detection windows widths that are established using these reference values can be reduced. Components for accurate analyses have been assembled in the past and here the construction of an accurate ion mobility spectrometry drift tube is described that is accurate to 0.1% of the calculated K_0 value and can be hermetically sealed without inserting the drift tube into a large vacuum chamber. Having a pressure sealed accurate ion mobility spectrometer will allow for the control of the pressure variable within the K_0 equation and the safe analysis of hazardous chemicals. Here the construction of an inexpensive and easily reparable sealed drift tube is described.

Keywords Accuracy · Precision · Calibration · False alarms · Hermetically sealed

✉ Brian C. Hauck
brian.c.hauck3.ctr@mail.mil

[1] Department of Chemistry, Washington State University, 305 Fulmer Hall, Pullman, WA 99164, USA

[2] Present address: ORISE Postdoctoral Fellow - U.S. Army Edgewood Chemical Biological Center, Aberdeen Proving Ground, Aberdeen, MD 21010, USA

[3] LEIDOS – U.S. Army Edgewood Chemical Biological Center Operations, P.O. Box 68, Gunpowder, MD 21010, USA

[4] Present address: Science and Technology Corporation (STC) – U.S. Army Edgewood Chemical Biological Center Operations, Gunpowder, MD 21010, USA

[5] U.S. Army Edgewood Chemical Biological Center, Aberdeen Proving Ground, Aberdeen, MD 21010, USA

Introduction

Ion mobility spectrometry (IMS) has become a heavily relied upon analytical technique for the detection of chemical warfare agents, narcotics, and explosives at international borders, aviation security checkpoints, and in active combat zones. By 2006, more than 50,000 IMS units were adopted for use in the field [1, 2]. The current accuracy of these field units is estimated to be, at best, ± 2% of the reduced mobility (K_0) value used to detect suspect agents [3, 4]. This level of accuracy leads to false positive alarms, wherein the instrument reports the presence of a compound of interest (COI) when it is in fact absent. This results in the loss of time and money as resources are diverted to verify the alarm. Field instruments are required to have false positive alarm rates below 5% to minimize the wasting of resources and even lower requirements on false negative responses to prevent the loss of life [5]. The majority of IMS-based commercial field instruments do not advertise false alarm rates, but two that do are the Hardened MobileTrace® (HMT) from Rapiscan Systems (previously

Morpho Detection Trace Detection division) and the Multi-Mode Threat Detector (MMTD) from Smiths Detection. The HMT and MMTD advertise false alarm rates of less than 2% and less 1%, respectively [6, 7]. In 2016 the United States Transportation Security Administration (TSA) screened more than 2 million airline passengers per day [8]. While it is unknown how many of those passengers were screened using IMS-based technology, if it is assumed that only 10% of all passengers were screened using IMS a false positive alarm rate of 2% still amounts to 4000 false alarms every day for United States commercial aviation alone.

The equations used during the detection process are shown in Eqs. (1) and (2).

$$K_0 = \frac{L^2}{Vt_d}\left(\frac{273.15}{T}\right)\left(\frac{P}{760}\right) \tag{1}$$

$$\frac{(K_{0std})t_{dstd}}{t_{dCOI}} = \frac{C_i}{t_{dCOI}} = K_{0COI} \tag{2}$$

In Eq. (1), the library of reference K_0 values in the literature are calculated from the length of the drift region (L), the voltage drop (V) and drift time (t_d) across L, and the temperature (T) and pressure (P) of the drift gas. The K_0 value of the COI ($K_{0\ COI}$) in Eq. (2) can be calculated using an instrument factor (C_i) specific for the instrument being used. The C_i is the product of a reference standard's measured drift time ($t_{d\ std}$) on a specific field instrument and the reference standard's previously determined K_0 value ($K_{0\ std}$) from Eq. (1), at the same operational parameters as the instrument. The C_i of the instrument is then divided by the measured drift time of the mobility peak of interest ($t_{d\ COI}$) to calculate $K_{0\ COI}$. If $K_{0\ COI}$ falls within a preprogramed detection window, determined through past reference measurements of the COI, a positive alarm is triggered [9–14].

The ±2% accuracy of field instruments is the product of a limitation in this COI detection method that relies on the accuracy of "known" reference K_0 values. The literature contains K_0 values of various potential reference standards [4, 14], to be used as $K_{0\ std}$, and of various COIs such as explosives [4, 15–23] and chemical warfare agent related compounds [9, 13, 24–27] to establish the detection windows. However, Eq. (2) is only as effective as the accuracy of the K_0 values used within it. Disagreement between the reported K_0 values of identical COI ions under similar conditions causes the need for wide detection windows in field instruments. These windows can only be as narrow as ±2% because of the error that produces this disagreement and they are often wider to eliminate false negative responses. The width of detection windows cannot be arbitrarily decreased to eliminate false positive alarms because the error that is propagated through Eq. (2) when calculating $K_{0\ COI}$ may result in a value that falls outside of the narrower window. The resulting false negative response may lead to injury or loss of life after the detonation of an explosive or release of a chemical agent past the security checkpoint. Therefore, the only way to decrease false positive alarms without inadvertently increasing false negative responses is to increase the accuracy of the literature K_0 values used by field instruments. If the accuracies of K_0 values for COIs are increased by an order of magnitude to ±0.2% the width of the detection windows can be decreased by a similar order of magnitude. These narrower windows can also be shifted to their correct positions based on the accurate characterization of COI responses to environmental changes such as drift gas water content [28]. Operators can then ensure that a true COI peak stays within the narrower window by using accurate values of $K_{0\ std}$ in Eq. (2) which will lower the propagation of error in the $K_{0\ COI}$ calculation. To measure accurate K_0 values for reference standards and COIs, each of the variables within Eq. (1); L, V, t_d, P, and T, need to be accurately and precisely measured and controlled so as to reduce the error that is propagated through both equations. Measuring and controlling these variables to within ±0.2% error allows the accuracy of K_0 values referenced by field instruments to be similarly improved by an order of magnitude to ±0.2%.

The two objectives of this study were to: first construct an accurate ion mobility instrument (AIMI) drift tube capable of measuring K_0 values to 0.2% accuracy or better based on accurately and precisely measured parameters, and second, hermetically seal the drift tube using simple methods. The ability to accurately measure instrumental parameters, and thus K_0 values, will enable the accurate calibration of other IMS instruments, and hermetically sealing the drift tube will enable pressure variation as well as the accurate and safe analysis of toxic chemicals as opposed to just their simulants, precursors, or degradation products. Previous low-pressure instruments that were sealed were expensive to construct due to the use of bulky vacuum chambers and electrical feedthroughs for high voltage power and low voltage sensory equipment attached to the drift tube. Commercial equipment and procedures required to use that equipment for accurate and precise control of the variables in Eq. (1) have been described for a previous IMS drift tube of a deposited electrode design [29]. However, accurate K_0 values were unable to be measured due to a crack in the drift tube that most likely caused electric field inhomogeneity. Here the construction details of a stacked-ring drift tube that is capable of accurate ion mobility measurements is described as well as the process by which it was hermetically sealed without using a vacuum chamber.

Experimental

Accurate measurement and precise control of variables

Commercial components and procedures for accurately measuring and controlling each of the five variables in Eq. 1 have been described in detail previously [29].

Time-of-flight mass spectrometer (*tof*MS)

The AIMI drift tube was interfaced to a *time-of-flight* mass spectrometer (*tof*MS) (Ionwerks, Inc.; Houston, TX) to mass identify all drift time peaks. The *tof*MS vacuum interface had a 300 μm pinhole and had a pressure of 1.6 Torr. Past the vacuum interface, the focusing region had a pressure of 2.5×10^{-2} Torr through which the ions passed and were then orthogonally extracted into the V-shaped flight path of the *tof*MS. The flight path had a pressure of 1.7×10^{-6} Torr. The *tof*MS had a microchannel plate detector in a chevron stack orientation (Photonis; Sturbridge, MA), and the pumps used were DS 102 and DS 602 rotary vane vacuum pumps, and V 75 and V 250 turbo pumps (Agilent Technologies Vacuum Products Division; Lexington, MA). Software developed at Ionwerks Inc. and run on the IDL Virtual Machine Platform (Harris Geospatial Solutions; Broomfield, CO) was used to generate spectra.

General construction of the accurate ion mobility instrument (AIMI) drift tube

Drift rings

The AIMI drift tube consisted of ceramic insulator and metal electrode rings. The insulator rings were made out of alumina (99.8%, Al_2O_3) (Morgan Technical Ceramic; Allentown, PA) and had an i.d. of 60.5 mm, an o.d. of 69 mm, and a width of 7 mm. The electrode rings were machined from Alloy 46 (National Electronic Alloys; Oakland, NJ), a nickel-iron Alloy (46% Ni). Alloy 46 was used because its coefficient of thermal expansion (7.5 ppm/°C) closely matched that of alumina (7.4 ppm/°C). The electrode rings, shown in the dimetric computer assisted design (CAD) drawing of Fig. 1a, had an i.d. of 58.5 mm, an o.d. of 66.5 mm, and a width of 8 mm. The electrode rings were machined to feature a small stepped face on each of their front and back faces; shown in the cross-sectional drawings of Fig. 1b and in detail in Fig. 1c. The stepped face was created by a 0.5 mm × 0.9 mm (width × height) ridge extruding from either side of a 2 mm wide central rim. From either side of this 0.5 mm ridge, the electrode portion of the part extended another 2.5 mm. This stepped face served to maintain a face-to-face contact between adjacent rings while creating a cavity into which ceramic adhesive would be injected in a later step. By injecting ceramic adhesive in this manner the known length of the drift tube was not altered by an unknown thickness of adhesive between rings, and the rings remained parallel so that the homogeneity of the electric field was maintained. A 1.45 mm diameter × 10 cm long threaded rod was screwed into a hole at the top of each electrode ring's central rim, which served as an electrode post and connection to the voltage divider through pin connectors (Positronic Industries Inc.; Springfield, MO).

When the ring portions of the electrodes were fitted within the i.d. of the insulator rings, the faces of the insulator rings made contact with the faces of the 0.5 mm ridge on the electrode rings. Fig. 2a shows three electrodes and three insulator rings. This left a 0.5 mm wide cavity between the insulator ring and the face of the central rim on the electrode, as well as a distance of 3 mm between insulator rings, as shown in detail in Fig. 2b. One electrode ring in both the reaction and drift regions of the AIMI drift tube was specially machined to feature a hollow electrode post for the insertion of T100–250 temperature probes, coupled to an F200 precision thermometer (Isotech; Colchester, VT), to enable the direct measurement of the drift gas temperature. When the temperature probes were not inserted, the hollow electrode post in the reaction region served as the sample introduction port.

Bradbury-Nielson ion gates

The AIMI drift tube contained two Bradbury-Nielson (BN) ion gates, which were used to initiate drift time measurements. Both BN ion gates were constructed using existing methods within this laboratory. Two BN ion gates were used to designate the length of the drift tube as the distance between them. The drift time of the ion therefore directly correlated to this length by measuring the drift time of the ion from each BN ion gate separately. During drift time measurements, whichever BN ion gate was not being used to gate ions was connected to its reference point on the drift tube resistor chain with wire and alligator clips. The difference between these two drift time measurements produced the time the ion took to travel between each BN ion gate; an accurately measured length [29]. Each BN ion gate consisted of a single ceramic insulator ring cut in half radially. A 1.25 mm wide channel was ground into the outer face of each half ring. One side of the channel was also ground down to have an o.d. of 66.2 mm. The smaller o.d. faces of the two BN ion gate halves were then cemented together with an array of parallel 0.003 in. o.d. Alloy 46 wires (California Fine Wire Company; Grover Beach, CA) spaced between them on 0.005 in. centers. Alternating wires were electrically connected to create two interleaved sets of parallel and electrically isolated wires.

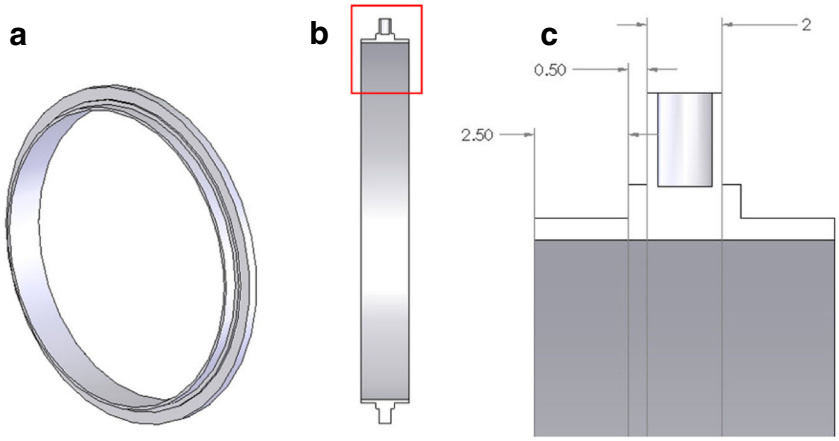

Fig. 1 CAD drawings of an **a** Alloy 46 electrode ring; **b** cross section of the Alloy 46 electrode ring; and **c** detailed view of the stepped face cross section highlighted by the red box in Fig. 1b. Dimensions are in mm

Ni-63 ionization source

Ni-63 was used to ionize the sample. The ion source was constructed to maintain a hermetic seal and confine the equipotential lines of the drift field to the interior of the drift tube. The ionization source base and its interface were designed to be modular and allow for ease in designing and installing new ionization sources such as corona discharge. The Ni-63 ionization source base and interface are shown in Fig. 3a. The ion source base was made of Alloy 46 and had four ceramic rods mounted to it. A wire mesh screen and cup holding a Ni-63 foil was mounted to the other end of the rods using small stubs attached to the base and Ni-63 cup. This ion source base screwed into the ionization source interface and compressed an alloy 718 C-seal (Jetseal, Inc.; Spokane, WA) for vacuum sealing. The ionization source interface sat against the front face and inside of a piece of 43.5 mm long alumina tubing with the same o.d. and i.d. as the alumina insulator rings. On the other side of this alumina piece was the first electrode ring of the AIMI drift tube, with a wire mesh screen spot welded to its front. The screen served to shield the equipotential lines within the drift tube from the grounded base plate of the ionization source. This established straight and vertical equipotential lines to keep the ions on a straight path towards the detector. Both the ion source base and the first electrode were machined to create a 0.5 mm cavity (identical to the ones described in Fig. 2b) between them and the long alumina piece. When the ion source base was screwed into the ion source interface, as shown in Fig. 3b, the ceramic rods on the base pushed the screen attached to the Ni-63 containing cup against the screen of the first electrode. This created electrical contact and supplied high voltage to the Ni-63 foil to induce ionization.

Drift gas showerhead

The last electrode before the *tof*MS vacuum interface served to introduce the neutral counter current flow of drift gas. This electrode also contained a Faraday plate for optional standalone analyses without the *tof*MS as the detector. The drift gas was introduced using a "showerhead" design. The drift gas showerhead/Faraday plate assembly, shown in Fig. 4, was placed behind the second gate and just before the pressure interface of the *tof*MS. It consisted of a central annular Faraday plate cemented within a piece of insulating alumina tubing using Resbond 920 fast curing ceramic adhesive (Cotronics Corp.; Brooklyn, NY). The alumina tubing holding the Faraday plate was likewise cemented within the i.d. of the drift gas entry showerhead.

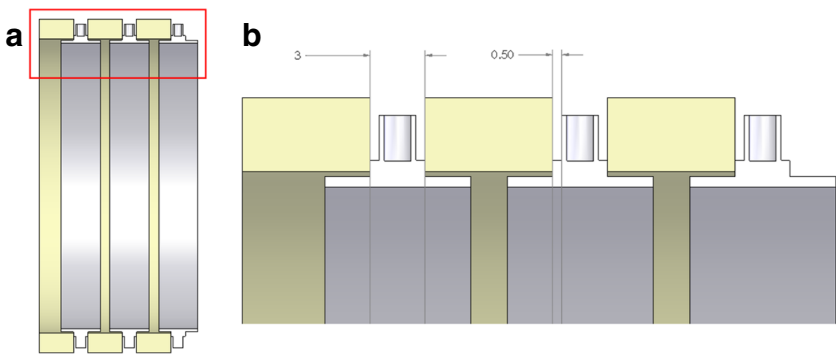

Fig. 2 CAD drawings of **a** cross-sectioned view of a stacked ring assembly consisting of three Alloy 46 electrodes (gray) and three ceramic insulator rings (tan); and **b** detailed view of the spacing of the drift rings highlighted by the red box in Fig. 2a

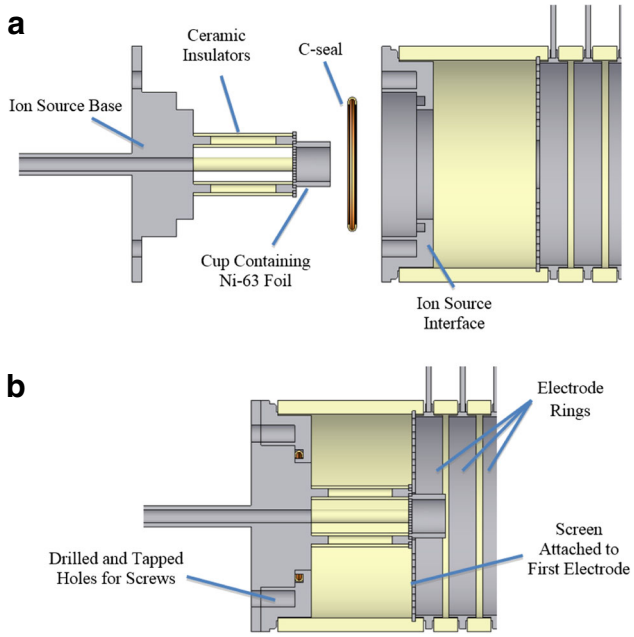

Fig. 3 CAD drawing of the ionization source base, C-seal, and interface **a** separated and **b** joined together to make electrical contact between the Ni-63 cup and first electrode screen as well as compressing the C-seal between the ionization source base and interface

On top of the showerhead, three different leads were seated. The first was a metal to ceramic brazed isolator on the left (Solid Sealing Technology, Inc.; Watervliet, NY). This isolator was hollow and it allowed for the attachment of a drift gas line using 1/8 in. Swagelok fittings and kept the line electrically isolated form the voltage applied to the showerhead. The next two leads were placed on the right and were in line with one another along the axis of the drift tube. The lead in front was a BNC cable attached to a 1 kV feedthrough (Solid Sealing Technology, Inc.). The other end of the feedthrough was spot welded to the backside of the Faraday plate to complete the circuit for standalone Faraday plate analyses. The last lead behind the BNC cable lead was the threaded rod screwed into the showerhead to supply voltage. The overall o.d. of the showerhead was the same as the ceramic insulator rings, and its front face was machined to create a 0.5 mm cavity identical to the ones described in Fig. 2b when placed against the second gate.

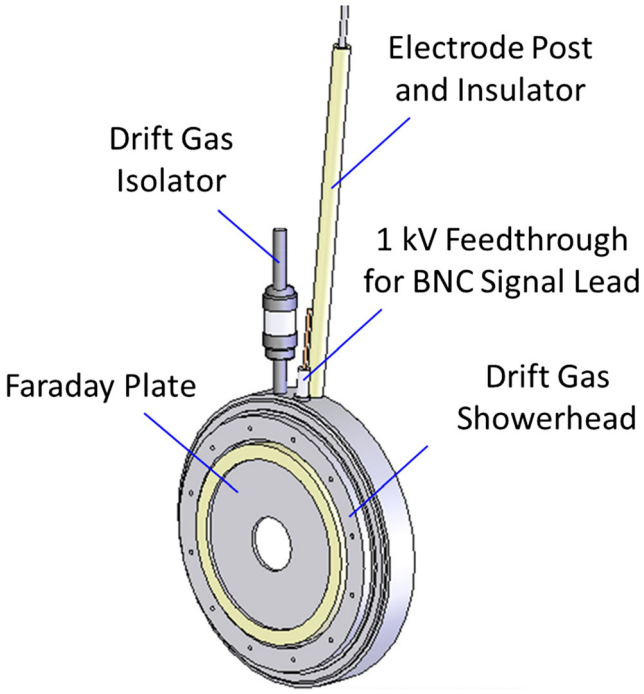

Fig. 4 CAD drawing of the drift gas showerhead assembly showing the Faraday plate and insulating ceramic cemented in the center, and the drift gas isolator, feedthrough for the BNC signal lead, and electrode post supplying voltage on top of the showerhead base

Pressure sealing procedure

Drift ring joints

To pressure seal each of the joints between the electrode and insulator rings, the two sections of the drift tube with continuous i.d.'s (the reaction and drift regions, excluding the BN ion gates) were mounted separately onto an adjustable mandrel that was tightly clamped down onto the mounted stack. The mandrel served to keep all drift rings in place during construction and ensure that the electrode rings were concentric and parallel to maintain a homogenous electric field. Resbond 920 fast curing ceramic adhesive was injected into the 0.5 mm cavities created by the machined ridges previously described. The ceramic adhesive was allowed to air dry for 24 h and then each region was then taken off the mandrel and heat cured in an oven at 150 °C for an additional 24 h. A light layer of Durapot 801 ceramic potting material (Cotronics) was then applied to the cured cement to help strengthen the joints. Similarly, the layer of Durapot 801 was allowed to air dry and then heat cured. After heat curing the Durapot 801, a layer of Celvaseal liquid vacuum leak sealant (Myers Vacuum; Kittanning, PA) was brushed onto the joints and allowed to air dry for 2 weeks.

After drying, each part was again placed in the oven to melt away excess Celvaseal and cure any that had permeated into the micropores of the ceramic. The parts were then cleaned of excess Celvaseal using dichloromethane and cotton tipped applicators. This left a layer of Celvaseal cured within the micropores of the drift tube joints. A second layer of Durapot 801 was then applied to the dried layer of Celvaseal to encase the vacuum seal layer. Special care was taken to ensure that the second layer of Durapot 801 did not extend past the o.d. of the ceramic insulator rings. Parts that were unable to be mounted on the mandrel (the BN ion gates, showerhead, first electrode, and ionization

source interface) were lined up within the rest of the assembly on the bench top and a 36 in. bar clamp was used to fasten the stack to the bench top. This ensured a tight mating of all faces and prevented the rings from separating when the ceramic adhesive was injected into the remaining joints. The same sealing procedure was then repeated for the remaining joints. The pressure seal was periodically tested during the construction process using a vacuum stage attached to a large rotary vane pump and an analog pressure gauge until the desired pressure was achieved.

Front and back end of the drift tube

The front end of the drift tube was sealed by the 39.7 mm o.d. × 34.5 mm i.d. C-Seal (Fig. 3). The C-Seal was compressed by screwing down the ion source front plate using eight socket cap screws. Four springs (McMaster-Carr Supply Company; Robbinsville, NJ), each with a force of 19 lbs./ft., were mounted equidistantly around four of the screws on the ion source front plate and compressed between the ion source front plate and the front plate of the thermal case holding the AIMI drift tube assembly. These springs pushed the AIMI drift tube up against the front of the *tof*MS and compressed a 2.25 in. i.d. x-profile double sealing o-ring (McMaster-Carr) that was placed around a seating ridge on the back of the drift gas showerhead. This double sealing o-ring created a pressure seal between the back of the showerhead and the front of the *tof*MS vacuum interface. A ceramic ring embedded in the back of the showerhead prevented the showerhead from making contact with the grounded interface housing in case the o-ring was over-compressed. The entire assembly is depicted by the dimetric cross-section illustrated in the CAD drawing in Fig. 5. The AIMI drift tube is shown housed within an insulating ceramic tube, which was in turn housed within the aluminum thermal case built in-house at WSU. The thermal case was attached to the *tof*MS vacuum interface using screws and thumb nuts.

Temperature probe and sample entry ports

The specialized electrode rings that allowed for the insertion of the temperature probes and sample also needed to be pressure sealed while still being able to easily connect to the pin connectors of the resistor chain. An EZRU21 external/internal reducing union (Valco Instruments Inc. Co.; Houston, TX) and a 1/8 in. Swagelok cap were modified to do so. A small hole was drilled and tapped into each fitting, on the side of the Valco fitting and on top of the Swagelok cap, without going through to the i.d. A small piece of a threaded rod was screwed into the hole onto which a male pin connector was soldered. The Valco external/internal reducing union was used on the electrode in the

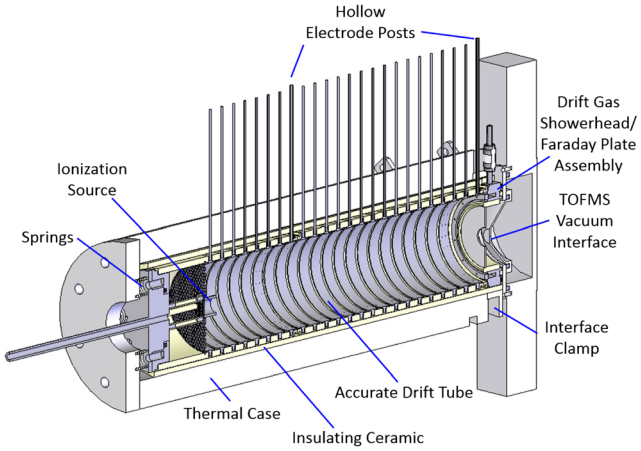

Fig. 5 Dimetric cross-section CAD drawing of constructed ion mobility spectrometer. Two hollow electrode posts before each gate allow for the insertion of temperature probes to directly measure the temperature of the drift gas as well as the introduction of sample through the first hollow electrode post

reaction region to allow for sample introduction into the drift tube through a silica capillary held by an FS1.36 fused silica adapter (Valco Instruments). The 1/8 in. Swagelok cap was used on the electrode ring in the drift region.

Ambient and reduced pressure operation

Compressed air was introduced as the drift gas at a rate of 1.00 ± 0.01 L/min using an 1179A digital mass flow controller, and a 640A pressure controller established non-ambient pressures (MKS instruments; Andover, MA). The mass flow and pressure controllers were powered and set by a 247D four-channel power supply and display (MKS instruments). The gas outlet of the IMS instrument was connected to a DS 42 dual stage rotary vane vacuum pump (Agilent Technologies Vacuum Products Division). The vacuum pump was turned on and an orifice within the pressure controller restricted the flow of gas evacuating from the drift tube to establish the pressure set on the 247D power supply and read out. The vacuum pump was disconnected from the gas outlet when conducting ambient pressure studies.

Chemicals

2,6-Di-*tert*-butyl pyridine (D*t*BP) and dimethyl methylphosphonate (DMMP) were both obtained as 97% pure standards (Sigma-Aldrich Chemical Co.; Houston, TX). 2,4,6-trinitrotoluene (TNT) was obtained as a 5 mg/mL stock solution in methanol (AccuStandard; New Haven, CT), and the stock solution was further diluted using HPLC grade methanol (Fisher Scientific; Waltham, MA) to create a 0.1 mg/mL sample solution. Aqueous ammonia was used to create a positive mode drift gas dopant for DMMP spectra and

was obtained in the form of Dynacal permeation tubes (Valco Instruments Inc. Co.). Two permeation tubes (10.6 cm long, 0.64 cm diameter each) inserted in-line with the drift gas created a nominal dopant concentration of 10 ppm when passed over with a flow of air at 1.000 ± 0.002 L/min and 23.4 °C.

Sample introduction

Headspace vapor samples of D*t*BP or DMMP were introduced into the instrument by pipetting 0.5 μL of neat sample in a 1/8 in. Swagelok cap and attaching the cap to the bottom of an 8 in. length of stainless steel tubing. The sample tee was connected to a compressed air gas tank on one side using Swagelok fittings and to a 250 μm i.d. × 360 μm o.d. fused silica capillary (Polymicro Technologies; Phoenix, AZ) on the other side using Valco fittings. The capillary was inserted through the specialized temperature probe port and terminated in the reaction region in the center of the drift tube diameter. The capillary was held in place in the temperature probe port by the Valco fitting, adapted for electrical continuity. The orthogonal flow of gas carried the headspace vapors rising from the sample tee through the silica capillary and into the reaction region of the AIMI drift tube. A 15 kV ceramic isolator (Solid Sealing Technology, Inc.) ensured electrical isolation of the drift tube from the sample gas line.

TNT was introduced into the AIMI drift tube by drawing an aliquot of the sample solution into a 17 cm silica capillary (150 μm i.d., 360 μm o.d) using a 250 μL gastight number 1725 (Hamilton Company; Reno, NV) syringe and Valco fittings. The solvent was evaporated for 1 h before attaching the capillary to the sample line using external/internal reducing unions (Valco Instruments Inc. Co.). A compressed air tank was operated at 20 psi to carry the explosive vapor into the reaction region of the AIMI drift tube.

Results and discussion

Assessment of accuracy

The first objective of this study was evaluated by performing an error analysis on the AIMI drift tube. Previously, Crawford et al. performed an error analysis on a stacked ring IMS-*tof*MS instrument with similar components to this instrument, reporting an accuracy of ±0.5% [4]. A similar error analysis was performed on the AIMI drift tube using typical instrumental parameter measurements, and their associated error, that were obtained for the five variables in Eq. (1) using procedures previously described [29]. The results of this error analysis for the AIMI drift tube are shown in Table 1.

Propagating the error associated with each variable in Table 1 produces an error of ±0.001 $cm^2\ V^{-1}\ s^{-1}$ for a K_0 value of 1 and ±0.002 $cm^2\ V^{-1}\ s^{-1}$ for a K_0 value of 2, amounting to an optimized error of ±0.1% for K_0 value measurements. Accurate K_0 values were also measured on the AIMI drift tube and compared to values produced by previous drift tubes. Table 2 shows the progression of K_0 values for D*t*BP and TNT at approximately 100 °C and 50 °C, respectively, collected on the previous stacked ring drift tube constructed by Crawford et al. [4], the drift tube of a metal deposition design and accurate components constructed by Hauck et al. [29], and the results reported by the current AIMI drift tube.

Within Table 2, the K_0 values of D*t*BP and TNT ions continually increased as new and more accurate instruments were constructed. This trend was seen for all ions studied, including those not reported here. Improvements in the design of the AIMI drift tube culminated in the production of accurate K_0 values that were up to 5% higher than values produced by other drift tubes that also had the aim of accurately analyzing COIs and potential reference standards [4, 11, 29]. When sources of error were eliminated or reduced between the stacked ring drift tube and the metal deposition drift tube through lower output ripple power supplies, lower temperature gradients, and two BN ion gates, the K_0 values of ions increased by approximately 4%. However, the metalized drift tube had a crack in the drift region that most likely introduced inhomogeneity into the electric field. When the homogeneity of the electric field was ensured through the construction of the AIMI drift tube, the K_0 values of ions increased by approximately an additional 1% and 0.4% for D*t*BP and TNT, respectively.

The K_0 values reported by Crawford et al. on the stacked ring drift tube were an average of twenty-four measurements across four electric field strengths ranging from 372 V/cm to 530 V/cm [4]. The electric field strengths corresponding to the values measured on the metal deposition drift tube were 400 V/cm for D*t*BP and 260 V/cm for TNT [29]. The electric field strengths corresponding to the values reported for the AIMI drift tube were 400 V/cm for D*t*BP and 280 V/cm for TNT. The slightly lower percent increase in TNT's K_0 value reported within Table 2 between the metal deposition and AIMI drift tubes, compared to D*t*BP's, is most likely the result of the K_0 values being measured at two different electric field strengths. If the K_0 value of TNT were measured at 280 V/cm on the less accurate metal deposition drift tube, instead of at 260 V/cm, the K_0 value would most likely have been slightly lower than the reported 1.564 $cm^2\ V^{-1}\ s^{-1}$. This would be due to a recently discovered phenomenon in which lower electric field strengths produced slightly higher K_0 values [30]. A higher percent increase in that hypothetical K_0 value at 280 V/cm on the metalized drift tube would then be seen when comparing it to the value measured at 280 V/cm on the AIMI drift tube.

The overall trend seen in Table 2 of increasing K_0 values with higher accuracy is a result of using values

Table 1 Error associated with each variable when calculating K_0 values and the source of each error, at 50.21 ± 0.04 °C and 280 V/cm, on the current AIMI drift tube

Variable (units)	Error	Source of largest error
L (cm)	$S_L = \frac{0.007\ \text{cm}}{16.252\ \text{cm}} = 4 \times 10^{-4}$	Calipers
V (V)	$S_V = \frac{0.2\ \text{V}}{4533.1\ \text{V}} = 4 \times 10^{-5}$	High Voltage Divider Probe and Digital Multimeter
t_d (s)	$S_{t_d} = \frac{1\times10^{-9}\ \text{s}}{1\times10^{-2}\ \text{s}} = 1 \times 10^{-7}$	*tof*MS clock rate
T (K)	$S_T = \frac{0.04\ \text{K}}{323.36\ \text{K}} = 1 \times 10^{-4}$	Drift Gas Temperature Gradient
P (Torr)	$S_P = \frac{0.2\ Torr}{690\ Torr} = 3 \times 10^{-4}$	Mercury Barometer

in Eq. 1, for the previous instruments, which would have otherwise been too low in the numerator or too high in the denominator. For example a geometrically measured drift length will be lower than the true length traveled by the ion in IMS-*tof*MS studies employing a single BN-ion gate. The measured L would be too low and the value of t_d would be too high due to the indirect correlation of the two variables. Voltage may be corrected for current drawdown at the measurement point [29, 30], but in doing so it is also important to use directly measured values of the resistors on the drift tube and in the high voltage divider probe. If nominal values of each are used and are higher than direct measurements, the value of V will be too high. Finally, if temperature gradients in the drift gas are not minimized or if the temperature of the drift gas is not directly measured [31], a value of T higher than in actuality may be used. Each of these situations will cause a decrease in the calculated K_0 value compared to if the true values for those variables were used.

Pressure sealing the drift tube

The second objective of this study was evaluated by periodically checking the ability of the AIMI drift tube components to hold an internal vacuum during construction and by operating the instrument under reduced pressure after final assembly. Before the final assembly step, in which the separate drift tube sections were cemented together, the BN ion gates, the drift region, and the reaction region were separately tested for their ability to maintain an internal vacuum. Each BN ion gate was able to achieve an internal pressure of 0.01 Torr and the drift and reaction regions were each able to achieve an internal pressure of 0.02 Torr. Upon completion of the drift tube construction and installation onto the *tof*MS, the DS42 vacuum pump was attached to the drift gas outlet but left in the off position and with no drift gas flowing into the drift tube. The *tof*MS pinhole alone was able to evacuate the AIMI drift tube to 69 Torr, and the pressures within the two-stage *tof*MS vacuum interface also decreased from 1.7 and 3.5×10^{-2} Torr to 3.0×10^{-1} and 9.9×10^{-3} Torr, respectively. When the vacuum pump was turned on while still keeping the drift gas flow off, the pressure within the drift tube further decreased to 10 Torr and the *tof*MS interface pressures decreased to 8.0×10^{-2} and 6.4×10^{-3} Torr. Such a vacuum is more than sufficient to obtain desired pressures down to 0.5 atm to conduct pressure experiments and also ensure the safe execution of experiments involving hazardous chemicals. The ability to conduct these sub ambient experiments was further demonstrated when the mass flow and pressure controllers were able to achieve a drift gas flow rate of 1 L/min and an internal pressure of 200 Torr, respectively.

Table 2 Increases in K_0 values of two ions on three consecutive drift tube designs toward accurate measurements on the AIMI drift tube

Drift tube	K_0 value (drift gas temperature) $cm^2\ V^{-1}\ s^{-1}$	
	D_tBPH^+	$(TNT\text{-}H)^-$
Stacked-ring	1.400 (96.9 ± 0.6 °C)	1.500 (49.1 ± 0.5 °C)
Metal deposition	1.457 (100.10 ± 0.03 °C)	1.564 (50.07 ± 0.01 °C)
AIMI	1.471 (100.13 ± 0.02 °C)	1.571 (50.21 ± 0.04 °C)

The performance of the instrument was tested under reduced pressures by collecting spectra of DMMP at 202 Torr. Fig. 6 shows a reduced pressure spectrum of DMMP compared to a DMMP spectrum taken at an ambient pressure of approximately 697 Torr. The *tof*MS confirmed that both pressure conditions produced the same reactant and product ions. The three drift time peaks corresponded to the proton-bound dimer of ammonia [$NH_3(NH_4)^+$, *m/z* 35], the ammoniated monomer of DMMP [$DMMPNH_4^+$, *m/z* 142], and the ammonium-bound dimer of DMMP [$(DMMP)_2NH_4^+$, *m/z* 266]. These product ions also produced fragment ions in the *tof*MS vacuum interface identified as ammonium [NH_4^+, *m/z* 18], the protonated monomer of DMMP [$DMMPH^+$, *m/z* 125], and the proton-bound dimer of DMMP [$(DMMP)_2H^+$, *m/z* 249]. At reduced pressure, the

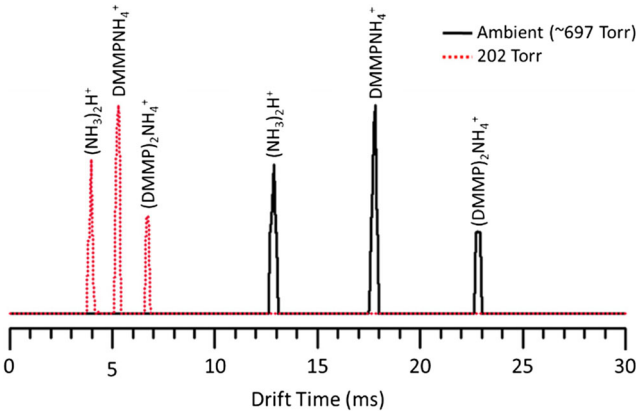

Fig. 6 Overlay mobility spectra of DMMP at ambient pressure (solid black trace) and reduced pressure (dashed red trace). Both spectra were taken at 425 V/cm and the drift gas had a moisture content of <5 ppm_v. As the pressure inside the IMS instrument was decreased, the drift time peaks shifted to faster drift times, higher resolving power, and lower resolution

resolution of the three peaks decreased as they shifted closer to one another and became sharper at 202 Torr. This demonstrates that the AIMI drift tube can be hermetically sealed and is operational at reduced pressures.

Conclusions

An accurate ion mobility instrument was constructed and can be used to measure K_0 values to ±0.1% based on the propagation of error in each of the variables within the K_0 equation. It is also possible to hermetically seal the instrument using a combination of design considerations, ceramic adhesive, and liquid vacuum sealant, both of which do not produce significant off gassing within the instrument. This process eliminates the need for high voltage feedthroughs and bulky vacuum chambers for the electrode rings. The ability to create a simple vacuum seal, and on an accurate instrument, will also enable the safe and accurate measurement of hazardous COIs' K_0 values. This design may be taken by other researchers and modified for their needs to accurately measure K_0 values of other COIs. The collection of accurate K_0 values can then also be aggregated to form a shared accurate database of mobilities for comparison and confirmation.

Acknowledgments Funding for this research was initially provided in part by Science Applications International Corporation, now LEIDOS, as a subcontract under a Task Order contract with U.S. Army Edgewood Chemical Biological Center and has been continued with the U.S. Army Research Office under grant #W911NF-12-1-0575. The construction of the IMS instrument would not have been possible without the expertise, skilled labor, and advice from Dave Savage, Lauren Frei, Steve Watson, and Fred Schutze of Washington State University's Technical Services Instrument and Electronics shops.

References

1. Eiceman GA, Stone JA (2004) Ion mobility spectrometers in National Defense. Anal Chem 76(21):390A–397A
2. Zulatov YA (2006) Ion mobility Speectrometry. J Anal Chem 61(6):519–519
3. Clemmer DE, Jarrold MF (1997) Ion mobility measurements and their applications to clusters and biomolecules. J Mass Spectrom 32:577–592
4. Crawford CL, Hauck BC, Tufariello JA, Harden CS, McHugh V, Siems WF, Hill HH Jr (2012) Accurate and reproducible ion mobility measurements for chemical standard evaluation. Talanta 101: 161–170
5. Buxton TL, Harrington P d B (2001) Rapid multivariate curve resolution applied to identification of explosives by ion mobility spectrometry. Anal Chim Acta 434(2):269–282
6. CBRNE Tech Index. http://www.cbrnetechindex.com/p/3330/Morpho-Detection-Inc/Hardened-MobileTrace-HMT. Accessed Oct 2017
7. CBRNE Tech Index. http://www.cbrnetechindex.com/p/4249/Smiths-Detection-Inc/MMTD-Multi-Mode-Threat-Detector. Accessed Oct 2017
8. TSA Year in Review: Record amount of Firearms Discovered in 2016. https://www.tsa.gov/blog/2017/01/12/tsa-year-review-record-amount-firearms-discovered-2016. Accessed Oct 2017
9. Kanu AB, Haigh PE, Hill HH Jr (2005) Surface detection of chemical warfare agent simulants and degradation products. Anal Chim Acta 553:148–159
10. Fernández-Maestre R, Harden CS, Ewing RG, Crawford CL, Hill HH Jr (2010) Chemical standards in ion mobility spectrometry. Analyst 135(6):1433–1442
11. Eiceman GA, Nazarov EG, Stone JA (2003) Chemical standards in ion mobility spectrometry. Anal Chim Acta 493:185–194
12. Ochoa ML, Harrington PB (2004) Detection of methamphetamine in the presence of nicotine using in situ chemical derivatization and ion mobility spectrometry. Anal Chem 76:985–991
13. Rearden P, Harrington PB (2005) Rapid screening of precursor and degradation products of chemical warfare agents in soil by solid-phase microextraction ion mobility spectrometry (SPME-IMS). Anal Chim Acta 545(1):13–20
14. Kaur-Atwal G, O'Connor G, Aksenov AA, Bocos-Bintintan V, Thomas CLP, Creaser CS (2009) Chemical standards for ion mobility spectrometry: a review. Int J Ion Mobil Spectrom 12:1–14
15. Spangler GE, Carrico JP, Campbell DN (1985) Recent advances in ion mobility spectrometry for explosives vapor detection. J Test Eval 13(3):234–240
16. Asbury GR, Klasmeier J, Hill HH Jr (2000) Analysis of explosives using electrospray ionization/ion mobility spectrometry (ESI/IMS). Talanta 50:1291–1298
17. Ewing RG, Miller CJ (2001) Detection of volatile vapors emitted from explosives with a handheld ion mobility spectrometer. Field Anal. Chem Technol 5(5):215–221
18. Ewing RG, Atkinson DA, Eiceman GA, Ewing GJ (2001) A critical review of ion mobility spectrometry for the detection of explosives and explosive related compounds. Talanta 54:515–529
19. Fetterolf DD (1993) Detection of trace explosive evidence by ion mobility spectrometry. In: Yinon J (Ed) Advances in Analysis and Detection of Explosives, Proceedings of the 4th international symposium on analysis and detection of explosives, Jerusalem, Israel, September 7–10, 1992. Kluwer Academic Publishers, Dordrecht, pp 117–132
20. Buttigieg GA, Knight AK, Denson S, Pommier C, Denton B (2003) Characterization of the explosive triacetone triperoxide and detection by ion mobility spectromtery. Forensic Sci Int 135:53–59

21. Tam M, Hill HH Jr (2004) Secondary electrospray ionization-ion mobility spectrometry for explosive vapor detection. Anal Chem 76:2741–2747
22. Lai H, Leung A, Magee M, Almirall JR (2010) Identification of volatile chemical signatures from plastic explosives by SPME-GC/MS and detection by ion mobility spectrometry. Anal Bioanal Chem 396:2997–3007
23. Crawford CL, Hill HH Jr (2013) Evaluation of false positive responses by mass spectrometry and ion mobility spectrometry for the detection of trace explosives in complex samples. Anal Chim Acta 795:36–43
24. Asbury GR, Wu C, Siems WF, Hill HH Jr (2000) Separation and identification of some chemical warfare agent degradation products using electrospray high resolution ion mobility spectrometry with mass selected detection. Anal Chim Acta 404:273–283
25. Steiner WE, Clowers BH, Matz LM, Siems WF, Hill HH Jr (2002) Rapid screening of aqueous chemical warfare agent degradation products: ambient pressure ion mobility mass spectrometry. Anal Chem 74:4343–4352
26. Steiner WE, Klopsch SJ, English WA, Clowers BH, Hill HH Jr (2005) Detection of a chemical warfare agent simulant in various aerosol matrixes by ion mobility time-of-flight mass spectrometry. Anal Chem 77:4792–4799
27. Steiner WE, Harden CS, Hong F, Klopsch SJ, Hill HH Jr, McHugh VM (2006) Detection of aqueous phase chemical warfare agent degradation products by negative mode ion mobility time-of-flight mass spectrometry [IM(tof)MS]. J Am Soc Mass Spectrom 17:241–245
28. Hauck BC, Davis EJ, Clark AE, Siems WF, Harden CS, McHugh VM, Hill HH Jr (2014) Determining the water content of a drift gas using reduced ion mobility measurements. Int J Mass Spectrom 368:37–44
29. Hauck BC, Siems WF, Harden CS, McHugh VM, Hill HH Jr (2016) *E/N* effects on K_0 values revealed by high precision measurements under low field conditions. Rev Sci Instrum 87:075104
30. Hauck BC, Siems WF, Harden CS, McHugh VM, Hill HH Jr (2017) Determination of *E/N* influence on K_0 values within the low field region of ion mobility spectrometry. J Phys Chem A 121:2274–2281
31. Fernández-Maestre F (2017) Calibration of the mobility scale in ion mobility spectrometry: the use of 2,4-lutidine as a chemical standard, the two-standard calibration method and the incorrect use of drift tube temperature for calibration. Anal Methods 9:4288–4292